Effects of stickiness in the classical and quantum ergodic lemon billiard

Črt Lozej ●,* Dragan Lukman ●,† and Marko Robnik ●‡

*CAMTP-Center for Applied Mathematics and Theoretical Physics, University of Maribor, Mladinska 3, SI-2000 Maribor,
Slovenia, European Union*

We study the classical and quantum ergodic lemon billiard introduced by Heller and Tomsovic in Phys. Today **46**(7), 38 (1993), for the case $B = 1/2$, which is a classically ergodic system (without a rigorous proof) exhibiting strong stickiness regions around a zero-measure bouncing ball modes. The structure of the classical stickiness regions is uncovered in the S-plots introduced by Lozej [Phys. Rev. E **101**, 052204 (2020)]. A unique classical transport or diffusion time cannot be defined. As a consequence the quantum states are characterized by the following *nonuniversal* properties: (i) All eigenstates are chaotic but localized as exhibited in the Poincaré-Husimi (PH) functions. (ii) The entropy localization measure A (also the normalized inverse participation ratio) has a nonuniversal distribution, typically bimodal, thus deviating from the beta distribution, the latter one being characteristic of uniformly chaotic systems with no stickiness regions. (iii) The energy-level spacing distribution is Berry-Robnik-Brody (BRB), capturing two effects: the *quantally divided phase space* (because most of the PH functions are either the inner-ones or the outer-ones, dictated by the classical stickiness, with an effective parameter μ_1 measuring the size of the inner region bordered by the sticky invariant object, namely, a cantorus), and the *localization of PH functions* characterized by the level repulsion (Brody) parameter β. (iv) In the energy range considered (between 20 000 states to 400 000 states above the ground state) the picture (the structure of the eigenstates and the statistics of the energy spectra) is not changing qualitatively, as β fluctuates around 0.8, while μ_1 decreases almost monotonically, with increasing energy.

I. INTRODUCTION

Quantum chaos, or more generally wave chaos, is an established field of research in physics [1–3]. The existence of dynamical chaos in quantum mechanics is still a subject of current debates. The sensitive dependence of time evolution (solution of time dependent Schrödinger equation) as an analogy of classical chaos certainly does not exist, because the overlap of two initial states remains rigorously constant due to the unitary time evolution. Also, of course, the analogy of classical orbits does not exist in quantum mechanics due to the Heisenberg uncertainty principle. Usually the quantum systems have a classical correspondent. If not, then a classical correspondent can be constructed and studied by means of introducing the coherent states, as is done—for example—in the Dicke model (see Ref. [4] and references therein). In the following we refer to quantum systems that have classical Hamiltonian correspondents.

The stationary quantum chaos is a well-established analogy of the classical chaos in Hamiltonian systems [1–3]. Namely, we find phenomena in the solutions of the time independent Schrödinger equation which correspond exactly to the classical structures. Such signatures of classical chaos are found in the statistical properties of the energy spectra, in the structure

of corresponding eigenfunctions and of their Wigner functions [5] or Husimi functions [6]. For example, the classically integrable systems exhibit Poisson statistics of the unfolded (reduced to unit mean level spacing) energy spectra, their wave functions have a well-ordered structure of nodal lines or surfaces, and their Wigner or Husimi functions are localized near the invariant tori in the classical phase space. However, in the opposite case of classically fully chaotic (ergodic) systems the energy spectra obey the statistics of random matrices, especially—but not only—of the Gaussian random matrices, the nodal patterns of eigenfunctions are entirely disordered and their probability amplitude exhibits a Gaussian random function [7]. Their Wigner or Husimi functions are ergodic, in the sense that they are on the average uniformly spread over the energy surface in the classical phase space. For a review see Refs. [3,8]. If the classical limit does not exist, then the above criteria can still be used as a definition of quantum chaos.

The above statements are valid under an important *semiclassical condition*, namely, that the dominating classical diffusion time or transport time t_T is sufficiently shorter than the Heisenberg time t_H, which by definition is $t_H = 2\pi\hbar/\Delta E$, where ΔE is the mean level spacing, or inverse energy-level density $\rho(E) = 1/\Delta E$ [9]. In such a case, if the semiclassical condition is satisfied, then all the above statements for fully chaotic systems have been proven to be rigorously true using the semiclassical methods, in particular, Gutzwiller's semiclassical theory of expressing the quantum Green function, and its trace $\rho(E)$, in terms of

---

*clozej@gmail.com
†dragan.lukman@gmail.com
‡Robnik@uni-mb.si

classical periodic orbits [10–14]. For fully chaotic systems, satisfying the semiclassical condition, this proof was initiated by Berry [15] in 1985, further developed by Sieber and Richter [16] in 2001, and completed by the group of Haake [17–20] in the years 2004–2010 [2]. Therefore, the well-known Bohigas-Giannoni-Schmit conjecture [21], initiated by Casati, Valz-Gris, and Guarneri [22], can be considered as proven.

Let us recall that the Heisenberg time goes to infinity when $\hbar$ goes to zero, because $\Delta E \propto \hbar^f$ and f is the number of degrees of freedom, $f \geqslant 2$, as we do not consider the systems having one degree of freedom. Thus, in the semiclassical limit $\hbar \to 0$, the Heisenberg time $t_H \propto \hbar^{1-f}$ eventually becomes larger than any classical transport time of the system t_T, as the latter one does not depend on $\hbar$. Their ratio,

$$\alpha = \frac{t_H}{t_T} = \frac{2\pi\hbar}{\Delta E \ t_T}, \tag{1}$$

is the important parameter characterizing the deepness of the semiclassical regime. Thus, the semiclassical condition is $\alpha \gg 1$. In such case the principle of uniform semiclassical condensation (PUSC) [8] of Wigner functions applies, saying that the Wigner functions become uniformly spread over the classical invariant component in the phase space, based on works by Percival [23], Berry [7], Shnirelman [24], Voros [25], and further developed by Veble, Robnik, and Liu [26]. This can be an invariant torus, a chaotic component, or the entire energy surface, depending on the dynamical properties and the structure of phase space (integrable, mixed-type or ergodic). Mixed-type systems have been studied for the first time in the context of quantum chaos by Berry and Robnik in 1984 [27]. Meanwhile, the literature on this problem has become quite extensive—for a recent review see Refs. [3,28].

If the semiclassical condition $\alpha \geqslant 1$ is not satisfied, then we observe localization properties of the chaotic eigenstates uncovered in the Wigner functions or Husimi functions in the phase space: The Wigner or Husimi functions are concentrated on a proper subset of the available classically chaotic region. In fact, the transition from strong localization at $\alpha \ll 1$ to strong delocalization at $\alpha \gg 1$ is a rather smooth one, as observed recently in several model systems. The chaotic regions in the classical Hamilton systems, either ergodic or of the mixed-type, can have strongly nonuniform "chaoticity": there are subregions that are more frequently visited by a chaotic orbit than the others, and this difference can vary over orders of magnitude. It can take a very long time to exit such a sticky region, and symmetrically, a long time to enter, if coming from outside. Such stickiness regions are bordered by cantori, which are invariant remnants of destroyed inviariant tori, with fractal dimension, and the size of their holes controls their permeability, and therefore the classical transport time. The quantification of the strength of the stickiness is characterized in Sec. II by the method of Lozej [29] in terms of the so-called S-plots. For the literature on stickiness, introduced by Contopoulos in 1971 [30], see the review by Meiss [31] and the references therein. To study these effects in an ergodic billiard system with strong stickiness is the main purpose of the present work, which follows a series of our recent papers [32–37]. As we shall see, stickiness implies nonuni-

versal behavior of the statistics of the energy spectra and of the localization measure.

In this paper we study a classically fully chaotic (ergodic) system, namely, a lemon billiard ($B = 1/2$) introduced by Heller and Tomsovic in 1993 [38], which possesses regions of strong stickiness, around the zero-measure bouncing ball invariant component, making its chaoticity strongly nonuniform. In this sense the system is nongeneric, not of a mixed-type, but still exhibiting features which in the quantum mechanics of the system imply nonuniversal, but very interesting behavior. We are facing and studying the consequences of the stickiness regions in the structure of eigenstates and of the corresponding energy spectra.

The paper is organized as follows. In Sec. II we define the family of lemon billiards, and describe its classical dynamical properties, showing that due to the strong stickiness regions the system is a nongeneric ergodic system. In Sec. III we study the corresponding quantum billiard and define the Poincaré-Husimi functions, and then explore their structure in correspondence with the structure of the classical phase space. In Sec. IV we define the entropy localization measure A and the normalized inverse participation ratio $R = nIPR$, showing that they are approximately linearly related, and then explore statistical properties of A. In Sec. V we analyze the statistical properties of the energy spectra, showing that the level spacing distribution is well described by the Berry-Robnik-Brody distribution (BRB), because due to the classical stickiness effects there is a region which quantum mechanics "sees" as an effective regular island whose relative size decreases almost monotonically with increasing energy. The chaotic part of the spectrum is subject to the Brody distribution with the level repulsion parameter β fluctuating around 0.8 with changing energy. In Sec. VI we present further comments regarding the interpretation of the results. Section VII presents the discussion, conclusions, and outlook.

II. THE DEFINITION OF THE LEMON BILLIARD ($B = 1/2$) AND ITS CLASSICAL DYNAMICAL PROPERTIES

The family of lemon billiards was introduced by Heller and Tomsovic in 1993 [38] and has been studied in a number of works [39–43], most recently by Lozej [29] and Bunimovich *et al.* [44]. The lemon billiard boundary is defined by the intersection of two circles of equal unit radius with the distance between their center $2B$ being less than their diameters and $B \in (0, 1)$, and is given by the following implicit equations in Cartesian coordinates:

$$(x + B)^2 + y^2 = 1, \quad x > 0,$$
$$(x - B)^2 + y^2 = 1, \quad x < 0. \tag{2}$$

As usual we use the canonical variables to specify the location s and the momentum component p on the boundary at the collision point. Namely, the arclength s counting in the mathematical positive sense (counterclockwise) from the point $(x, y) = (0, -\sqrt{1 - B^2})$ as the origin, while p is equal to the sine of the reflection angle θ, thus $p = \sin\theta \in [-1, 1]$, as $\theta \in [-\pi/2, \pi/2]$. The bounce map $(s, p) \Rightarrow (s', p')$ is area preserving as in all billiard systems [45]. Due to the two kinks the Lazutkin invariant tori (related to the boundary glancing

orbits) do not exist. The period-2 orbit connecting the centers of the two circular arcs at the positions $(1 - B, 0)$ and $(-1 + B, 0)$ is always stable (and therefore surrounded by a regular island) except for the case $B = 1/2$, the subject of our present work, where it is a marginally unstable periodic orbit (MUPO). One can see from the geometry that in our case $B = 1/2$ any orbit starting from middle of the circle will hit the other circle at the right angle and thus will retrace itself, because the centers exactly overlap with the arc of the other circle. This is true for all angles $|\theta| \leqslant \pi/3$ such that $-p_0 \leqslant p \leqslant p_0$, where $p_0 = \sqrt{3}/2 \approx 0.8660254$, and the particle hits the corner of the lemon billiard. Therefore, we have a line of MUPO as an one-dimensional invariant object in the phase space, namely, located at $s = \mathcal{L}/4$ and $s = 3\mathcal{L}/4$ on the intervals $p \in (-p_0, p_0)$, where $\mathcal{L}$ is the circumference of the entire billiard, for a general B equal to

$$\mathcal{L} = 4 \arctan \sqrt{B^{-2} - 1}. \tag{3}$$

and for $B = 1/2$ it is $\mathcal{L} = 4 \arctan \sqrt{3} = 4\pi/3 \approx 4.188790$. The area $\mathcal{A}$ of the billiard for a general B is equal to

$$\mathcal{A} = 2 \arctan \sqrt{B^{-2} - 1} - 2B\sqrt{1 - B^2}, \tag{4}$$

thus for $B = 1/2$ it is $\mathcal{A} = \frac{2\pi}{3} - \frac{\sqrt{3}}{2} \approx 1.2283697$. Of course, correspondingly, we have also invariant line of MUPO (we shall call them bouncing ball regions of period-4 orbits) in the phase space located at $p = 0$ and all s. It will be demonstrated that these bouncing ball regions are surrounded by a very strong stickiness region: even after 10^{11} bounces of a single chaotic orbit, starting at $(s = \mathcal{L}/2 + 0.0001, p = 0.999)$, there is still possibly a tiny unoccupied island around $s = \mathcal{L}/4$ and $s = 3\mathcal{L}/4$ and $p = 0$. But we believe that the system is ergodic, lacking a rigorous proof. The structure of the phase space after 10^6, 10^7, 10^8, 10^9, 5.10^9, and 10^{10} collisions emanating from the above initial condition is shown in Fig. 1.

In Fig. 2 we show the S-plot using the method introduced in Ref. [29], to quantify the stickiness in the phase space. In this approach the phase space is divided into a network of equal cells defined by the uniform grid of size L, in our case $L = 1000$, implying $L^2 = 10^6$ cells, and in each cell the distribution of the discrete return times τ (number of iterations/bounces) is observed, by calculating the mean value of the return time $\langle \tau \rangle$ and of the standard deviation σ. Their ratio is the quantity $S = \sigma/\langle \tau \rangle$. If the distribution of τ is Poissonian (exponential) characteristic of uniform chaoticity described by the random model [46], then we have $S = 1$, while in the case of stickiness we find distribution typically described by the superposition of several exponential distributions (so-called hyperexponential distribution) and $S > 1$. Figure 2 clearly shows extremely strong stickiness in the diamond shaped areas around $s = \mathcal{L}/4$ and $s = 3\mathcal{L}/4$ and $p = 0$, which has implications and manifestations in the quantum domain to be studied in the next sections.

Lemon billiards of other values of B are not considered in this paper, but have been treated classically in Ref. [29] and are subject of our forthcoming papers.
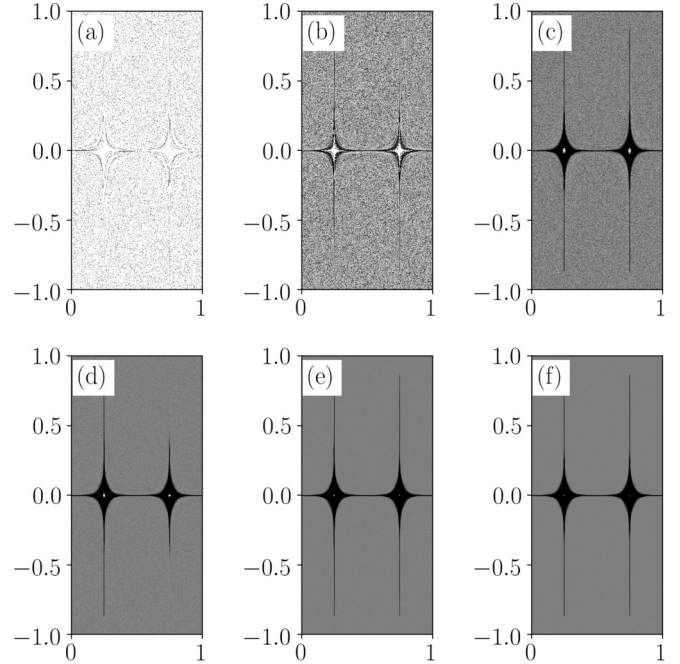

FIG. 1. The phase portrait as generated by a single chaotic orbit emanating from the same initial condition ($s = \mathcal{L}/2 + 0.0001$, $p = 0.999$) after 10^6, 10^7, 10^8, 10^9, 5×10^9, and 10^{10} collisions, from (a) to (f), respectively. The label on the abscissa is $s/\mathcal{L}$, while on the ordinate we have $p \in [-1, 1]$.

III. THE QUANTUM BILLIARD: THE HELMHOLTZ EQUATION AND THE POINCARÉ-HUSIMI FUNCTIONS

A. The Helmholtz equation

Quantum mechanically we have to solve the stationary Schrödinger equation, which in a billiard $\mathcal{B}$ is just the Helmholtz equation,

$$\Delta \psi + k^2 \psi = 0, \tag{5}$$

with the Dirichlet boundary conditions $\psi|_{\partial \mathcal{B}} = 0$. The energy is $E = k^2$. The important quantity is the boundary function

$$u(s) = \mathbf{n} \cdot \nabla_{\mathbf{r}} \psi[\mathbf{r}(s)], \tag{6}$$
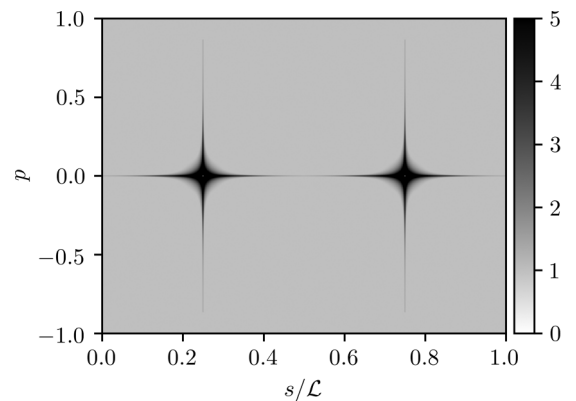

FIG. 2. The S-plot on a grid of cells 1000×1000, showing the extremely strong stickiness region around $s = \mathcal{L}/4$ and $s = 3\mathcal{L}/4$ and $p = 0$.

which is the normal derivative of the wave function ψ at the point s (**n** is the unit outward normal vector). It satisfies the integral equation

$$u(s) = -2 \oint dt \, u(t) \, \mathbf{n} \cdot \nabla_{\mathbf{r}} G[\mathbf{r}, \mathbf{r}(t)], \qquad (7)$$

where $G(\mathbf{r}, \mathbf{r}') = -\frac{i}{4} H_0^{(1)}(k|\mathbf{r} - \mathbf{r}'|)$ is the Green function in terms of the Hankel function $H_0^{(1)}(x)$. It is important to realize that the boundary function $u(s)$ contains complete information about the wave function at any point **r** inside the billiard by the equation

$$\psi_m(\mathbf{r}) = -\oint dt \, u_m(t) \, G[\mathbf{r}, \mathbf{r}(t)]. \qquad (8)$$

Here m is just the index (sequential quantum number) of the mth eigenstate.

The number of energy levels $\mathcal{N}(E)$ below $E = k^2$ is determined quite accurately, especially at large energies, asymptotically exact, by the celebrated Weyl formula (with perimeter corrections) using the Dirichlet boundary conditions, namely,

$$\mathcal{N}(E) = \frac{\mathcal{A} \, E}{4\pi} - \frac{\mathcal{L} \, \sqrt{E}}{4\pi} + \text{c.c.,} \qquad (9)$$

where c.c. are small constants determined by the corners and the curvature of the billiard boundary. Thus, the density of levels $\rho(E) = d\mathcal{N}/dE$ is equal to

$$\rho(E) = \frac{\mathcal{A}}{4\pi} - \frac{\mathcal{L}}{8\pi \sqrt{E}}. \qquad (10)$$

Our numerical solving the Helmholtz equation is based on the plane wave decomposition method and the Vergini-Saraceno scaling method [47,48]. The numerical accuracy has been checked by the Weyl formula, to make sure that we are neither losing levels nor getting too many due to the double counting (distinguishing almost degenerate pairs from the numerical pairs) in the overlapping energy intervals, and also by the convergence test. The number of missing levels or too many levels was never larger than 1 per 1000 levels (usually less than 10 per 10 000 levels).

Our billiard has two reflection symmetries, thus four symmetry classes: even-even, even-odd, odd-even, and odd-odd. For the purpose of analyzing the spectral statistics we have thus considered only the quarter billiard, while for the wave functions (and the corresponding PH functions) we have used the half billiard of odd symmetry.

B. The Poincaré-Husimi functions

Let us define the quantum phase space. One way is to calculate the Wigner functions [5] based on $\psi_m(\mathbf{r})$. However, in billiards it is more natural and convenient to calculate the Poincaré-Husimi (PH) functions, based on the boundary function Eq. (6). The Husimi functions [6] are Gaussian smoothed Wigner functions, which makes them positive definite. We can treat them as quasiprobability densities. Following Tualle and Voros [49] and Bäcker *et al.* [50], we introduce [33,34] the properly $\mathcal{L}$-periodized coherent states centered at (q, p), as

follows:

$$c_{(q,p),k}(s) = \sum_{m \in \mathbf{Z}} \exp\{i \, k \, p \, (s - q + m \, \mathcal{L})\}$$

$$\times \exp\left[-\frac{k}{2}(s - q + m \, \mathcal{L})^2\right]. \qquad (11)$$

The Poincaré-Husimi function is defined as the absolute square of the projection of the boundary function $u(s)$ onto the coherent state, namely,

$$H_m(q, p) = \left| \oint c_{(q,p),k_m}(s) \, u_m(s) \, ds \right|^2. \qquad (12)$$

All eigenstates are chaotic in the sense that the entire classical phase space (s, p) is chaotic, but not uniformly chaotic. Namely, due to the classical stickiness regions surrounding the bouncing ball regions (of MUPO) of Figs. 1 and 2 the PH functions are localized in various regions, as shown in Fig. 3: Some are strongly localized at the very center of the bouncing ball region, some are surrounding it inside the virtual boundary between the inner and outer part of the stickiness region, some are localized on this boundary, some are localized outside this boundary in a nonuniform way, and finally some are rather uniformly spread in the outside region, not penetrating into the inner region. All eigenstates and PH functions have been calculated for a half billiard, for the odd parity. In the following we perform the quantitative analysis of the degree of localization, by calculating the entropy localization measure A.

IV. THE LOCALIZATION MEASURES: THE ENTROPY LOCALIZATION MEASURE A AND THE NORMALIZED INVERSE PARTICIPATION RATIO NIPR

A. The definition of localization measure

The degree of localization can be quantified in at least three different ways: entropy localization measure A, correlation localization measure C, and the normalized inverse participation ration $R = nIPR$. We have shown [33,34,37] that they are linearly related and thus equivalent.

The *entropy localization measure* of a *single eigenstate* $H_m(q, p)$, denoted by A_m is defined as

$$A_m = \frac{\exp I_m}{N_c}, \qquad (13)$$

where

$$I_m = -\int dq \, dp \, H_m(q, p) \ln[(2\pi \hbar)^f H_m(q, p)] \qquad (14)$$

is the information entropy. Here f is the number of degrees of freedom (for 2D billiards $f = 2$, and for surface of section it is $f = 1$) and N_c is a number of cells on the classical chaotic domain, $N_c = \Omega_c/(2\pi \hbar)^f$, where Ω_c is the classical phase space volume of the classical chaotic component. In the case of the uniform distribution (extended eigenstates) $H = 1/\Omega_C = \text{const.}$ the localization measure is $A = 1$, while in the case of the strongest localization $I = 0$, and $A = 1/N_C \approx 0$. The Poincaré-Husimi function $H(q, p)$ (12) (normalized) was calculated on the grid points (i, j) in the phase space (s, p),
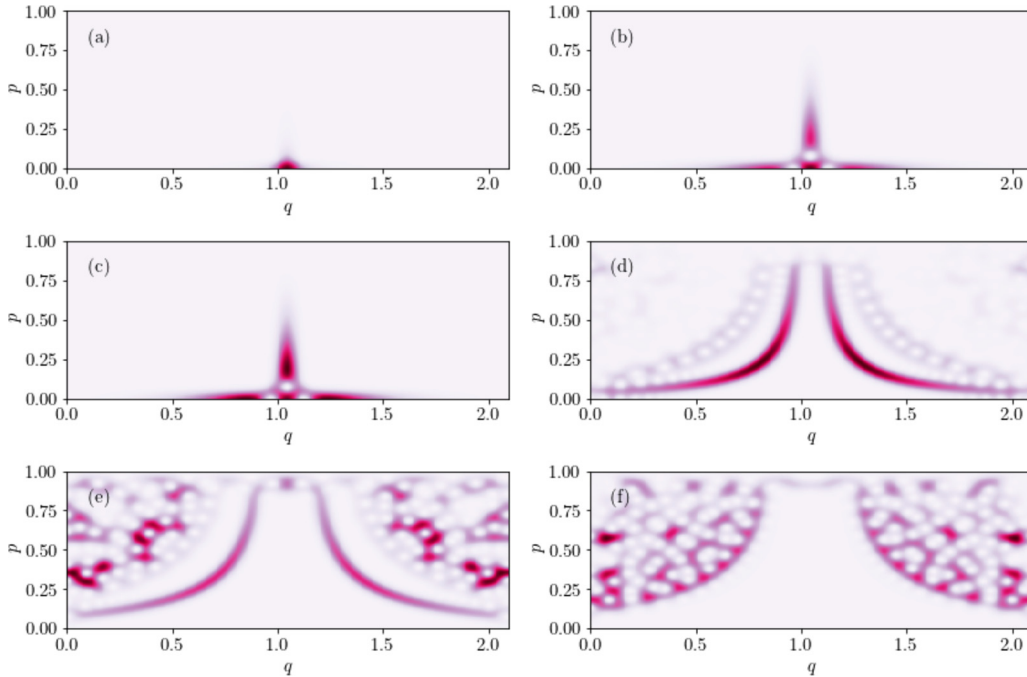
FIG. 3. Examples of typical Poincaré-Husimi functions at various k: 641.670665, 654.237553, 647.954107, 854.360748, 865.888129, and 858.033634 in (a)–(f), respectively. Their structure is strongly determined by the classical stickiness structures in Figs. 1 and 2. Due to the reflection and time reversal symmetries we plot only one quarter of the phase space. Higher color intensity corresponds to higher values of the PH function.

and we express the localization measure in terms of the discretized function. In our numerical calculations we have put $2\pi\hbar = 1$, and thus we have $H_{ij} = 1/N$, where N is the number of grid points, in case of complete extendedness, while for maximal localization we have $H_{ij} = 1$ at just one point, and zero elsewhere. In all calculations we have used the grid of 400×400 points, thus $N = 160\,000$.

As mentioned in the introduction, the definitions of localization measures can be diverse, and the question arises to what extent are the results objective and possibly independent of the definition. Indeed, in Ref. [33], it has been shown that A and C (based on the correlations) are linearly related and thus equivalent. Moreover, we have introduced [36,37] also the normalized inverse participation ratio $R = nIPR$, defined as follows:

$$R = \frac{1}{N} \frac{1}{\sum_{i,j} H_{ij}^2}, \qquad (15)$$

for each individual eigenstate m. Here the normalization $\sum_{ij} H_{ij} = 1$ has been done. However, because we expect fluctuations of the localization measures even in the quantum ergodic regime (due to the scars, etc.), we must perform some averaging over an ensemble of eigenstates, and for this we have chosen 20 consecutive eigenstates. The linear relation of $R = nIPR$ versus $\langle A \rangle$ has been clearly demonstrated in Refs. [36,37] for the stadium billiards and the mixed-type billiards (Robnik billiard [51,52]), while in the present work for the lemon billiard we find approximate agreement with the linear relationship, shown in Fig. 4.

Also, importantly, very recently we have shown that such a linear relationship is valid in the Dicke model. Its classical

analog based on coherent states is a Hamilton system with a smooth potential [4]. A similar finding was reported in Ref. [53] and references therein. Therefore, we believe that such relationship is generally true, independent of a specific model system (billiards or smooth potentials).

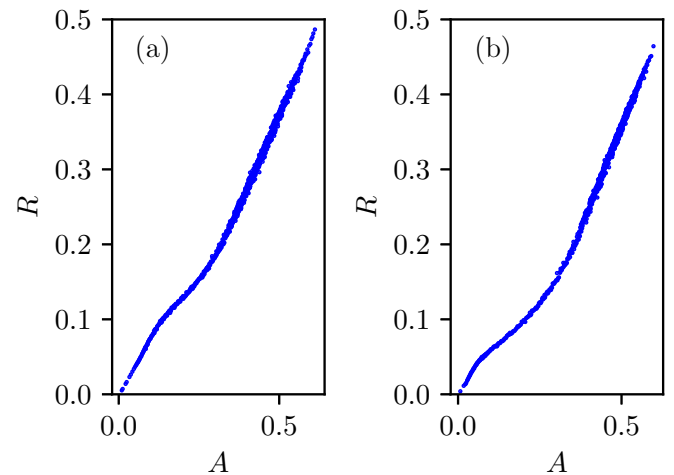In the following we shall use exclusively A as the measure of localization.

FIG. 4. The relationship between the normalized inverse participation ratio $R = nIPR$ and the entropy localization measure A averaged over the 20 consecutive Poincaré-Husimi functions, for the 20 000 consecutive eigenstates with k above $k_0 = 640$ (a) and $k_0 = 2880$ (b).

B. The distributions of the localization measures *A*

One of the main questions addressed in this paper are the statistical properties of *A*. In our previous works it has been shown that in the stadium (Bunimovich billiard) *A* obeys the beta distribution [37], while in the mixed-type Robnik billiard the beta distribution appears at sufficiently uniform chaoticity and sufficiently large energies [36]. In the case of the Dicke model it has also been found that *A* are distributed according to the beta distribution [4]. Thus, we believe that beta distribution of *A* is universally valid, provided that the stickiness regions and effects do not exist, so that we have uniform chaoticity (constant value of *S* in the *S*-plots introduced by Lozej [29]). Our aim in the present work is to clearly demonstrate the effects of stickiness in the quantum properties of classically chaotic Hamilton systems, in our case the lemon billiard $B = 1/2$.

The so-called *beta distribution* is

$$P(A) = CA^a (A_0 - A)^b, \qquad (16)$$

where A_0 is the upper limit of the interval $[0, A_0]$ on which $P(A)$ is defined, and the two exponents a and b are positive real numbers, while C is the normalization constant such that $\int_0^{A_0} P(A)\, dA = 1$, i.e.,

$$C^{-1} = A_0^{a+b+1} B(a+1, b+1), \qquad (17)$$

where $B(x, y) = \int_0^1 t^{x-1}(1-t)^{y-1}dt$ is the beta function. Thus, we have for the first moment

$$\langle A \rangle = A_0 \frac{a+1}{a+b+3}, \qquad (18)$$

and for the second moment

$$\langle A^2 \rangle = A_0^2 \frac{(a+2)(a+1)}{(a+b+4)(a+b+3)}, \qquad (19)$$

and therefore for the standard deviation $\sigma = \sqrt{\langle A^2 \rangle - \langle A \rangle^2}$

$$\sigma^2 = A_0^2 \frac{(a+2)(b+2)}{(a+b+4)(a+b+3)^2}, \qquad (20)$$

such that asymptotically $\sigma \approx A_0 \frac{\sqrt{b+2}}{a}$ when $a \to \infty$. In this limit $P(A)$ becomes Dirac δ function peaked at $A = A_0$.

In Fig. 5 we show a selection of typical distributions $P(A)$. We clearly see the nonuniversal bimodal distribution, deviating from the beta distribution, and this applies to all energies considered $E_0 = k_0^2$, namely, for $k_0 = 640, 920, 1200, 1480, 1760, 2040, 2320, 2600, 2880$.

Therefore, in Fig. 5 we show only the cases $k_0 = 640$ and $k_0 = 2880$, as in between there is no qualitative difference. The structure is similar to the structure of $P(A)$ in the mixed-type billiard (Robnik billiard) in the regime of strongly nonuniform chaoticity [36].

It should be noted that losing a few states, which can happen, does not affect the result for $P(A)$ in any significant way. Also, the statistical significance is very high, which has been carefully checked by using a (factor 2) smaller number of objects in all histograms, as well as by changing the size of the bins.

The limiting case $a \to \infty$ in Eqs. (18) and (20) comprising the fully extended states in the limit $\alpha \to \infty$ shows that the distribution tends to the Dirac δ function peaked
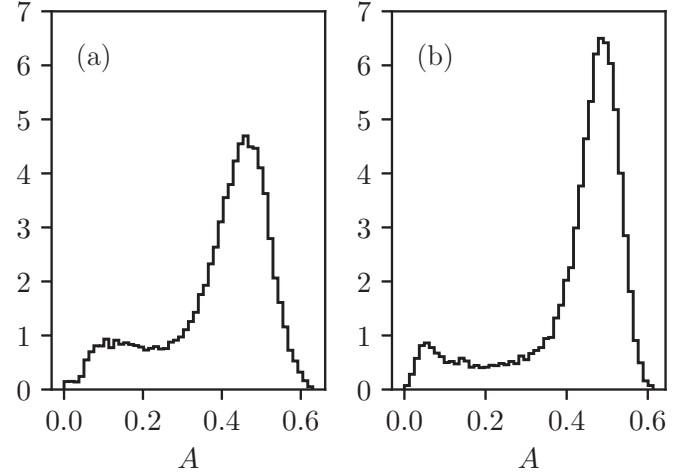

FIG. 5. The histograms of the distribution of the entropy localization measure $P(A)$ for 19 987 eigenstates above $k_0 = 640$ in (a), and for 19960 eigenstates above $k_0 = 2\,880$ in (b). The calculation is for the half billiard of odd parity.

at A_0, thus $\sigma = 0$ and $P(A) = \delta(A_0 - A)$, in agreement with Shnirelman's theorem [24], which is not observed in our case, but would appear at higher energies $E = k_0^2$. In our case the characteristic classical transport time t_T cannot be uniquely defined, as it varies widely with the location of the initial conditions with respect to the stickiness region. Nevertheless, we predict that for sufficiently high energies k_0^2 eventually all relevant classical transport times become sufficiently small. The Heisenberg time t_H is constant, and the semiclassical parameter α Eq. (1) for ergodic billiard is [33,34]

$$\alpha = \frac{t_H}{t_T} = \frac{\mathcal{L}\, k_0}{\pi\, N_T}, \qquad (21)$$

where N_T is the number of collisions associated with the transport time t_T. Thus, $\alpha \to \infty$ as $k_0 \to \infty$, and we need even higher energies to see this transition into the universal regime exhibiting the beta distribution for $P(A)$.

We have analyzed the PH functions of the states taken from the smaller peak around $A \approx 0.1$, and from the larger peak $A \approx 0.45$. In the first case we see strongly localized inner states, inside the stickiness region (Fig. 6), while in the second case the states are localized outside the stickiness region, either uniformly or nonuniformly (Fig. 7).

If we separate the states belonging to the two peaks, using some overlap criterion (taking only the PH functions that maximally overlap with the outer chaotic region), and thus consider only the family of states belonging to the larger peak, which "live" outside the stickiness region, then we find a unimodal distribution which is quite well described by the beta distribution as demonstrated in Fig. 8, characteristic of the systems and regimes with no stickiness (uniform chaoticity) as demonstrated in Refs. [36,37].

V. THE SPECTRAL STATISTICS: BERRY-ROBNIK-BRODY DISTRIBUTION

Now we turn to the spectral analysis, namely, the analysis of the level spacing distribution. For an introduction see
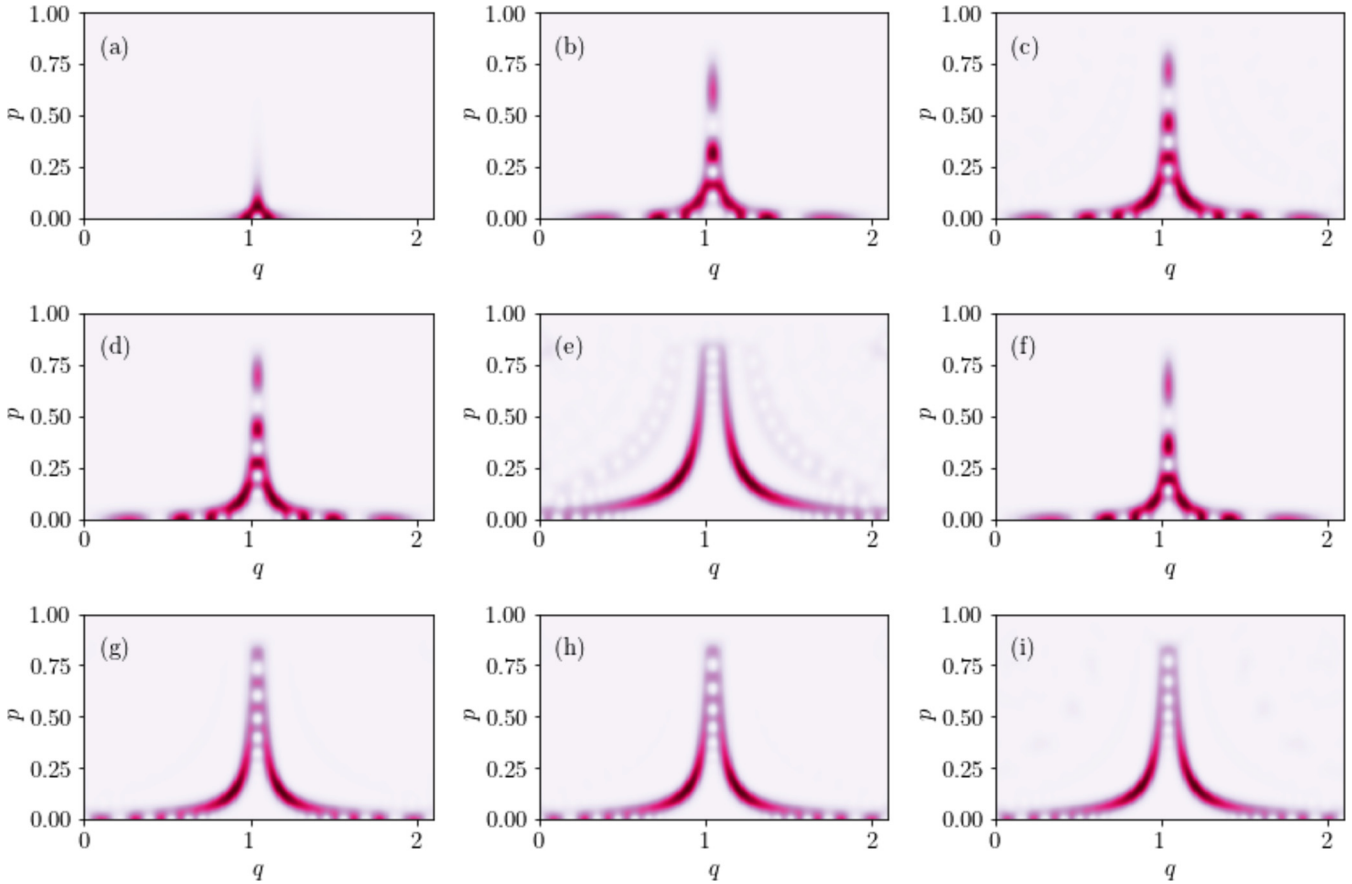
FIG. 6. Examples of the inner localized Poincaré-Husimi functions at various k: 643.241487, 646.390631, 657.395766, 699.804421, 714.221189, 718.648216, 754.840525, 764.290106, 803.599980, in (a)–(i), respectively. Their structure is strongly determined by the classical stickiness structures in Figs. 1 and 2. The calculation is for the half billiard of odd parity. Due to the reflection and time reversal symmetries we plot only one quarter of the phase space. Higher color intensity corresponds to higher values of the PH function.

Ref. [28]. Since the billiard is ergodic, one would expect the Brody distribution [54,55],

$$P_B(S) = cS^\beta \exp(-dS^{\beta+1}), \qquad (22)$$

where by normalization of the total probability and the first moment we have

$$c = (\beta + 1)d, \quad d = \left[\Gamma\left(\frac{\beta+2}{\beta+1} \right) \right]^{\beta+1}, \qquad (23)$$

with $\Gamma(x)$ being the Γ function. It interpolates the exponential and Wigner distribution as β goes from 0 to 1. The corresponding gap probability is

$$\mathcal{E}_B(S) = \frac{1}{\gamma(\beta+1)} Q\left(\frac{1}{\beta+1}, (\gamma S)^{\beta+1} \right), \qquad (24)$$

where $\gamma = \Gamma(\frac{\beta+2}{\beta+1})$ and $Q(a, x)$ is the incomplete Γ function,

$$Q(a, x) = \int_x^\infty t^{a-1} e^{-t} dt. \qquad (25)$$

The degree of localization which determines β is controlled by the parameter α Eq. (1). However, due to the effects of stickiness the classical transport time cannot be defined unambiguously, as it depends strongly on the location of the initial conditions in the phase space (s, p), and therefore so does α

as well. Due to the strong stickiness around the center of the bouncing ball region quantum mechanics "sees" effectively a hole, whose size decreases with energy, and thus this hole plays a role of a quasiregular region (the complement of the outer chaotic region) for most of the eigenstates, as has been demonstrated in the PH functions. The mechanism behind this phenomenon is the existence of a cantorus, or several cantori, which present a border between the inner and outer region. Namely, the holes of a cantorus are nonpermeable for the quantum mechanics (waves) if the flux is smaller than a Planck cell, but thus become permeable at higher energies (or smaller Planck constant $2\pi\hbar$) [48,56,57]. Therefore, we must expect that the level spacing distribution will be well described by the Berry-Robnik-Brody (BRB) distribution, with the two parameters, μ_1 measuring the relative size of the quasiregular region (and the relative density of the corresponding level sequence) and β measuring the strength of the localization of the chaotic part of the spectrum.

The BRB distribution is calculated as the second derivative of the gap probability $\mathcal{E}$,

$$P(S) = \frac{d^2\mathcal{E}}{dS^2}, \qquad (26)$$

where the total gap probability is the product of the regular (Poissonian part) $\mathcal{E}_P = \exp(-S)$ and of the chaotic
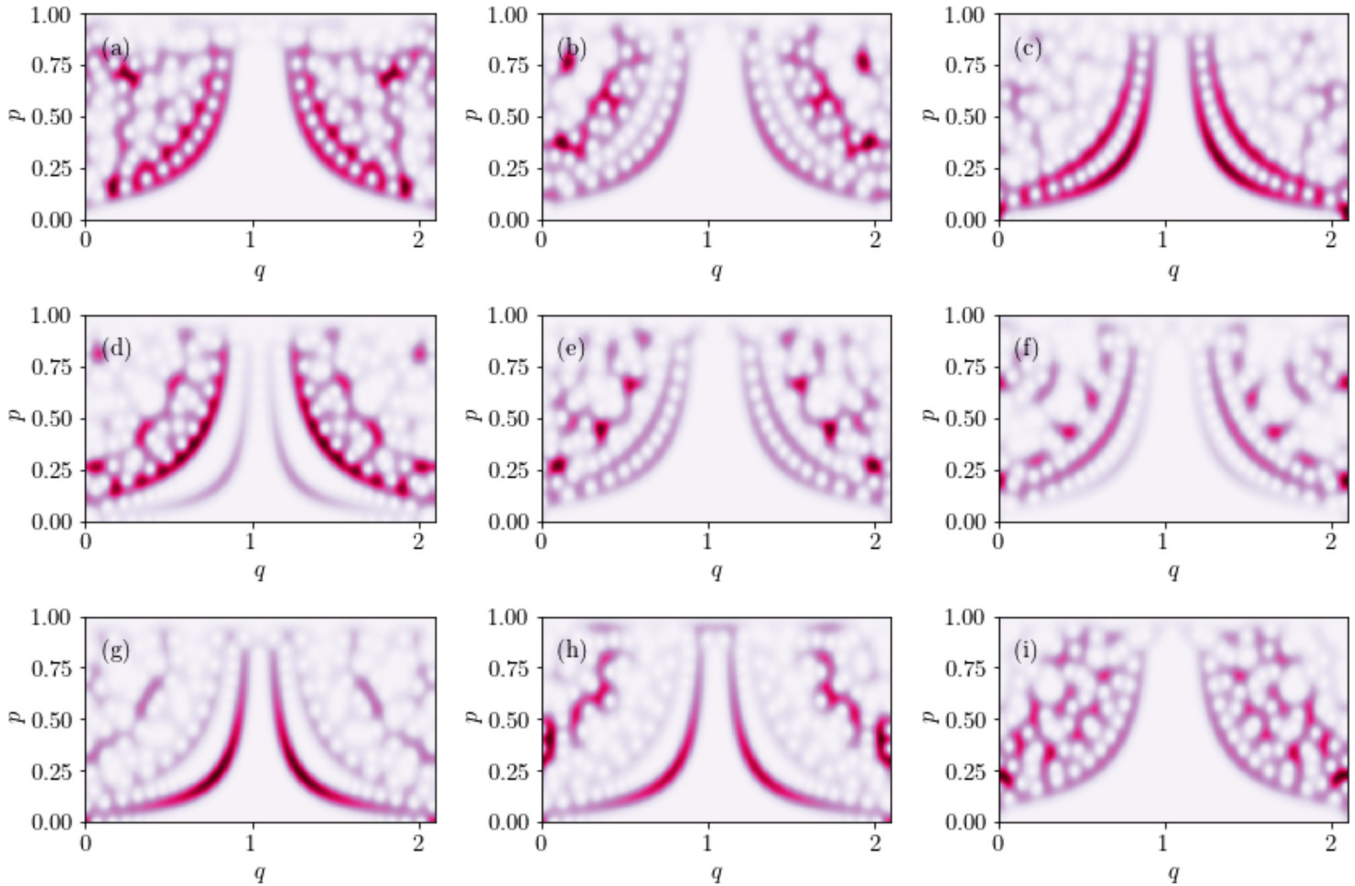
FIG. 7. Examples of the outer localized Poincaré-Husimi functions at various k: 645.621455, 645.653750, 645.989357, 646.691491, 646.835747, 647.615914, 648.527598, 648.609436, 650.435253 in (a)–(i), respectively. Their structure is strongly determined by the classical stickiness structures in Figs. 1 and 2. The calculation is for the half billiard of even parity. Due to the reflection and time reversal symmetries we plot only one quarter of the phase space. Higher color intensity corresponds to higher values of the PH function.
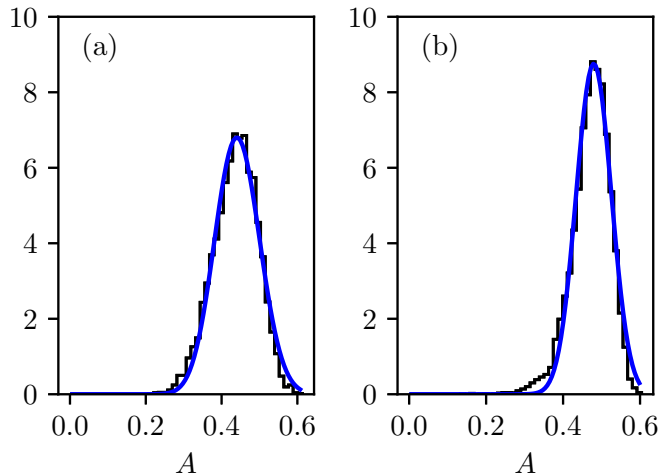

FIG. 8. The histograms of the distribution of the entropy localization measure $P(A)$ for 12 678 eigenstates above $k_0 = 640$ in (a), and for 15 571 eigenstates above $k_0 = 2880$ in (b). The distributions are quite well fitted with the β distribution with the parameters $(a, b) = (26.083, 31.531)$ in (a) and $(a, b) = (47.255, 50.399)$ in (b). The states have been selected by the criterion of maximal overlap with the outer chaotic region. The calculation is for the half billiard of odd parity.

part Eq. (24),

$$\mathcal{E}(S) = \mathcal{E}_P(\mu_1 S)\,\mathcal{E}_B(\mu_2 S) = \exp(-\mu_1 S)\,\mathcal{E}_B(\mu_2 S), \quad (27)$$

where $\mu_1 + \mu_2 = 1$. The resulting BRB distribution captures both effects, the quasidivided quantum phase space, and the localization on the outer chaotic component.

This expectation is excellently confirmed in our numerical calculations. It is observed that the value of β fluctuates around the value 0.8, depending on the symmetry class and the energy k_0^2, while μ_1 decreases almost monotonically with increasing energy k_0^2. At even higher energies, which we have not yet reached, β is expected to increase towards 1 and μ_1 to zero. In this limit both the division of the phase space and the localization effects disappear and we would find just GOE level spacing distribution, well approximated by the Wigner distribution, which is Brody distribution Eq. (22) at $\beta = 1$.

In Fig. 9 we show the level spacing distributions for nine energy intervals each starting at $k_0 =$ 640, 920, 1200, 1480, 1760, 2040, 2320, 2600, 2880 and comprising about 40 000 levels that include all four symmetry groups (about 10 000 levels of each symmetry group). They are all very well fitted by the Berry-Robnik-Brody distribution Eq. (26). Note that the value of $P(S = 0)$ monotonically decreases with increasing energy k_0, as predicted: At higher energies the quantum
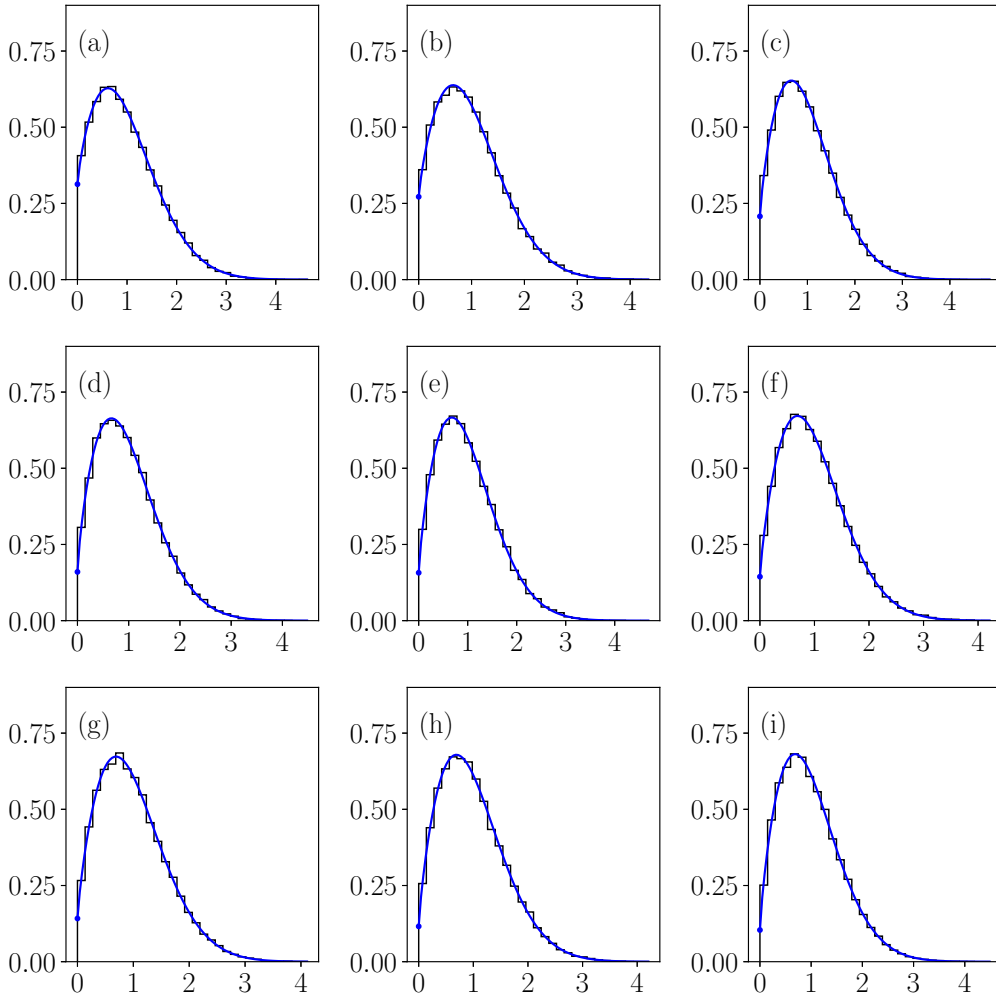
FIG. 9. The histograms of the level spacing distribution $P(S)$ for nine energy intervals each starting at $k_0 =$ 640, 920, 1200, 1480, 1760, 2040, 2320, 2600, 2880 and comprising about 40 000 levels that include all four symmetry groups (about 10 000 levels of each symmetry group) for each k_0. The fitting parameters (β, μ_1) are from (a) to (i): (0.827, 0.171), (0.844, 0.147), (0.806, 0.110), (0.778, 0.083), (0.799, 0.082), (0.813, 0.075), (0.816, 0.074), (0.801, 0.060), (0.789, 0.053). By the thick dot we denote the value of $P(S = 0)$, which decreases monotonically with increasing k_0.

resolution of the classical structures in the phase space increases, therefore the eigenstates tend towards the ergodic regime, in which the stickiness plays lesser and lesser role [μ_1 and $P(S = 0)$ tend to zero].

To verify the goodness of the BRB distribution we plot in Fig. 10 also the cumulative level spacing distribution for the case $k_0 = 640$, twofold, for the 1 000 consecutive eigenstates of the odd-odd parity in Fig. 10(b), and for the 39 965 eigenstates of all four parities in Fig. 10(a). We see very good agreement. It is seen that increasing the energy range and the number of levels significantly changes the values of β and μ_1 and the quality of the theoretical fitting BRB, although two effects work against each other: Increasing the energy range makes β less sharply defined while increasing the number of objects decreases the statistical error. We may conclude that the agreement is excellent.

In Fig. 11 we show the dependence of β on the energy k_0 for about 10 000 levels of each parity, and the collection of all four parities. It is seen that β fluctuates around 0.8. At still higher energies it is predicted to increase toward the value

$\beta = 1$ (Wigner distribution, which is 2-dim GOE), in the deep semiclassical limit.

In Fig. 12 we show the dependence of the parameter μ_1 on the energy k_0, for about 10 000 levels of each parity, and the collection of all four parities, clearly showing that it almost monotonically decreases with k_0. Asymptotically it must tend to zero, as the system is (practically) ergodic.

VI. ADDITIONAL COMMENTS

In the course of our present work we have widely explored the PH functions and the level spacing statistics by varying all possible parameters, like k_0, the number of levels n above k_0 from 1000 to 10 000 taken in histograms and cumulative level spacing distribution, the four parities, the size of the bins in histograms, etc. Hundreds of PH functions have been produced and analyzed, as well as hundreds of level spacing statistics, from plentiful different points of view.

The general conclusion is that the determination of the Berry-Robnik-Brody distribution is far from trivial and the
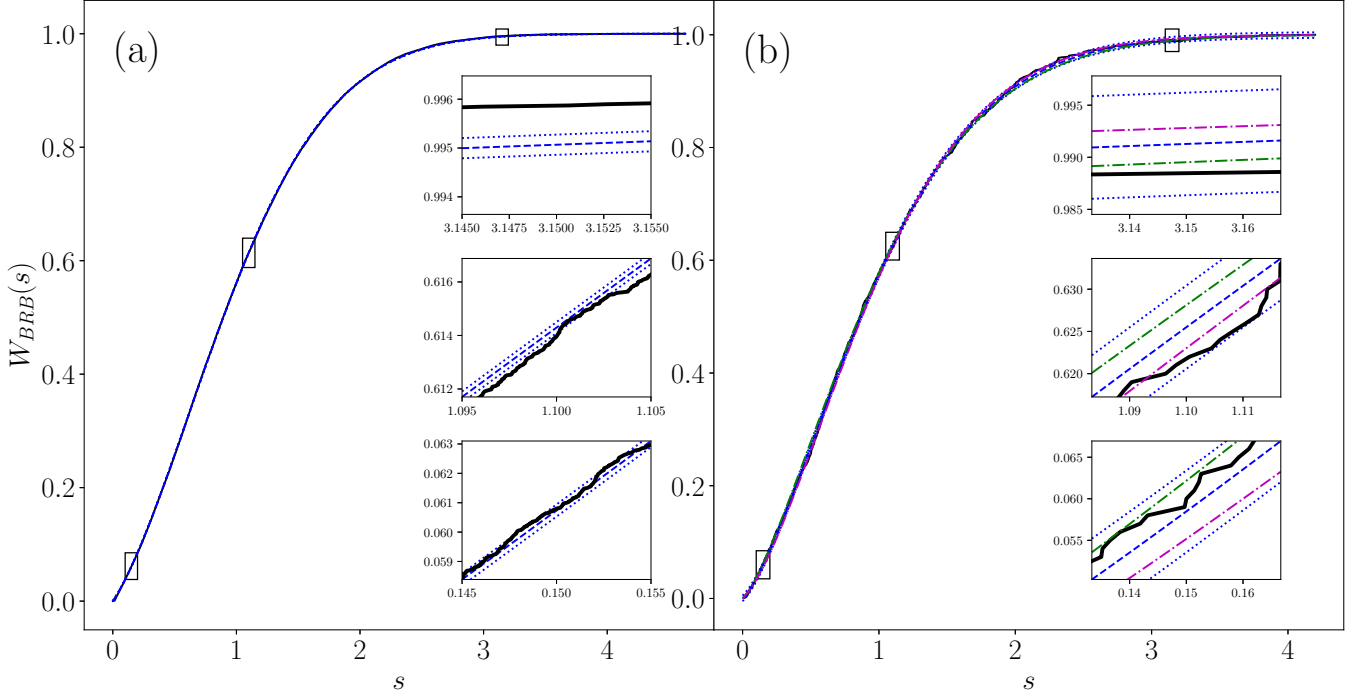
FIG. 10. The cumulative level spacing distribution $W(S)$ for two energy intervals each starting at $k_0 = 640$: in (a) 39 965 levels comprising all four parities, and in (b), 1000 levels of odd-odd parity. The parameters (β, μ_1) are $(0.827, 0.171)$ in (a) and $(0.569, 0.092)$ in (b). To display small deviation of data from the best fitting BRB distribution we show in the insets magnification: The thick lines (black) are the numerical data, the best fitting BRB curve is dashed (blue), the dotted (blue) lines designate the $\pm$ one standard deviation from the best fitting BRB curve, and the dash-dotted lines (magenta and green) denote the BRB curves with the same μ_1 but different β by the amount ± 0.05. One should observe the significantly different values of β and μ_1 compared between (a) and (b), showing that the statistics based on almost 40 000 levels (a) is better than in the case of only 1000 levels (b).

values of the parameters β and μ_1 depend quite sensitively on the above mentioned parameters. Of course, the most reliable data are the largest ones, comprising typically 10 000 levels per k_0 and parity, on which our conclusions are based.

Another remark concerns the classical transport time t_T or N_T (the number of collisions associated with t_T), which enters in the general expression for α in Eq. (1), and for a general ergodic billiard in Eq. (21). This time scale cannot

be uniquely defined, as its value depends strongly on the initial conditions. Nevertheless, a rough estimate has been done for initial conditions close to $p = 0$ (remember, the line $(s, p = 0)$ is invariant) with the result $N_T \approx 1000$. In our case $\mathcal{L} = 4\pi/3 = 4.188790$, therefore $\alpha \approx 4k_0/3000$, and in the range $k_0 \in [640, 2880]$ we have $\alpha \in [0.853, 3.84]$. This means that we are just in the middle of the localization transition region from $\alpha \ll 1$ to $\alpha \gg 1$, indicating that we should
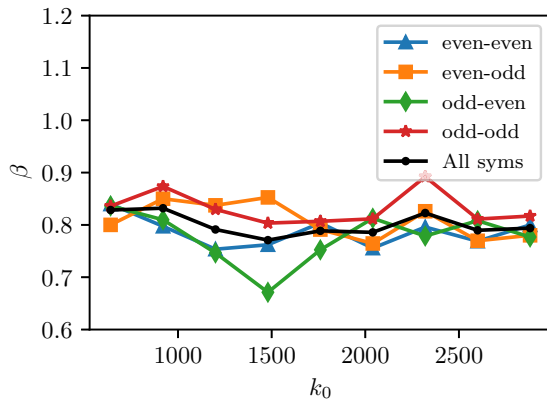

FIG. 11. The dependence of the β parameter on the energy k_0. For each k_0 we have taken about 10 000 states of given parity above k_0, and also show the data for the ensemble of all four parities. The value of β fluctuates around $\beta \approx 0.8$.
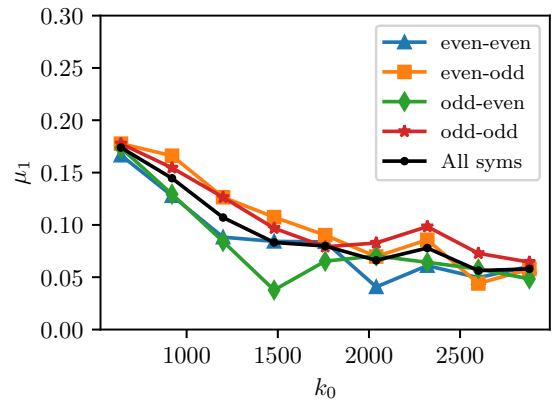

FIG. 12. The dependence of the μ_1 parameter on the energy k_0. For each k_0 we have taken about 10 000 states of given parity above k_0, and also show the data for the ensemble of all four parities. The value of μ_1 decreases almost monotonically with k_0.

see quite strongly expressed localization of PH functions, which is indeed the case. However, our energy interval $E = k_0^2$ with $k_0 \in [640, 2880]$ is too narrow to observe the variation of β with k_0, that is why β fluctuates around 0.8.

More precise estimates must be done by analyzing in detail the structure of the strong stickiness region, which implies at least two quite different time scales: One inside the sticky region, and the other outside. Quantum mechanically the boundary between them depends on the energy k_0^2. Such a more detailed analysis is left for the future.

VII. DISCUSSION AND CONCLUSIONS

We have presented the semiempirical analysis of the chaotic ergodic lemon billiard ($B = 1/2$), classically and quantally. The existence of strong stickiness regions around the invariant zero-measure bouncing ball lines as quantified by the phase portraits (density plots) and Lozej's S-plots has important consequences for the quantum mechanics of the same billiard. The Poincaré-Husimi (PH) functions are strongly localized and their entropy localization measure A has a bimodal distribution, qualitatively due to the existence of basically two PH functions populations, namely, the inside ones and the outside ones. If we eliminate the inner eigenstates, then we find that A obeys quite well the beta distribution characteristic for the uniform chaoticity (no stickiness in chaotic region and $S = 1$). The existence of such a strong stickiness region is manifested also in the energy spectral statistics. As the quantum mechanics "sees" the inner region, at given energy k_0^2, effectively as a separate regular region as the complement of the outer chaotic region, the level spacing distribution is Berry-Robnik-Brody (BRB) with two parameters: β measures the degree of localization and the level repulsion effect, and

μ_1 measures effectively the size of the inner sticky region. The agreement of data with BRB is excellent. As α is roughly within the interval $\alpha \in [0.853, 3.84]$, we see that β is hardly changing with the energy k_0^2, and fluctuates around 0.8, while the parameter μ_1 decreases almost monotonically with k_0, as predicted: The quantum resolution of the classical phase space structures increases with increasing energy. Asymptotically, when $k_0 \to \infty$ we predict $\beta \to 1$ and $\mu_1 \to 0$. However, to reach these higher energies, a major computational effort is necessary. A more detailed analysis of the structure of the stickiness region, the associated transport time scales and their quantum implications are left for the future, which requires calculation of eigenstates and PH functions at much higher energies.

Another still open problem is the theoretical explanation of the Brody level spacing distribution even in the case of uniformly chaotic (no stickiness) regime with localized PH functions. This includes the distribution of the entropy localization measure A as beta distribution.

These aspects have been explored and demonstrated in Refs. [33–37] in other billiards, and very recently by Wang and Robnik [4] also for the Dicke model, whose classical counterpart based on the coherent states is a Hamilton system with a smooth potential, which corroborates our findings. It seems that a semiclassical method based on Gutzwiller's periodic orbit theory [10–14] might be an appropriate approach [1,2] to solve this problem.

[1] H.-J. Stöckmann, *Quantum Chaos—An Introduction* (Cambridge University Press, Cambridge, UK, 1999).

[2] F. Haake, *Quantum Signatures of Chaos* (Springer, Berlin, 2001).

[3] M. Robnik, Eur. Phys. J. Spec. Top. **225**, 959 (2016).

[4] Q. Wang and M. Robnik, Phys. Rev. E **102**, 032212 (2020).

[5] E. Wigner, Phys. Rev. **40**, 749 (1932).

[6] K. Husimi, Proc. Phys. Math. Soc. Jpn. **22**, 264 (1940).

[7] M. V. Berry, J. Phys. A: Math. Gen. **10**, 2083 (1977).

[8] M. Robnik, Nonlinear Phenom. Complex Syst. (Minsk) **1**, 1 (1998).

[9] It has been pointed out to us that historically this concept has been used explicitly for the first time by Victor Weisskopf, although in the literature we are unable to trace this back.

[10] M. C. Gutzwiller, J. Math. Phys. **8**, 1979 (1967).

[11] M. C. Gutzwiller, J. Math. Phys. **10**, 1004 (1969).

[12] M. C. Gutzwiller, J. Math. Phys. **11**, 1791 (1970).

[13] M. C. Gutzwiller, J. Math. Phys. **12**, 1791 (1971).

[14] M. C. Gutzwiller, Phys. Rev. Lett. **45**, 150 (1980).

[15] M. V. Berry, Proc. Roy. Soc. Lond. A **400**, 229 (1985).

[16] M. Sieber and K. Richter, Phys. Scr. **2001**, 128 (2001).

[17] S. Müller, S. Heusler, P. Braun, F. Haake, and A. Altland, Phys. Rev. Lett. **93**, 014103 (2004).

[18] S. Heusler, S. Müller, P. Braun, and F. Haake, J. Phys. A: Math. Gen. **37**, L31 (2004).

[19] S. Müller, S. Heusler, P. Braun, F. Haake, and A. Altland, Phys. Rev. E **72**, 046207 (2005).

[20] S. Müller, S. Heusler, A. Altland, P. Braun, and F. Haake, New J. Phys. **11**, 103025 (2009).

[21] O. Bohigas, M. J. Giannoni, and C. Schmit, Phys. Rev. Lett. **52**, 1 (1984).

[22] G. Casati, F. Valz-Gris, and I. Guarneri, Lett. Nuovo Cimento **28**, 279 (1980).

[23] I. C. Percival, J. Phys B: At. Mol. Phys. **6**, L229 (1973).

[24] A. I. Shnirelman, Usp. Mat. Nauk **29**, 181 (1974).

[25] A. Voros, Lect. Notes Phys. **93**, 326 (1979).

[26] G. Veble, M. Robnik, and J. Liu, J. Phys. A: Math. Gen. **32**, 6423 (1999).

[27] M. V. Berry and M. Robnik, J. Phys. A: Math. Gen. **17**, 2413 (1984).

[28] M. Robnik, Nonlinear Phenom. Complex Syst. (Minsk) **23**, 172 (2020).

[29] Č. Lozej, Phys. Rev. E **101**, 052204 (2020).

[30] G. Contopoulos, Astron. J. **76**, 147 (1971).

[31] J. Meiss, Chaos **25**, 097602 (2015).

[32] B. Batistić and M. Robnik, J. Phys. A: Math. Theor. **43**, 215101 (2010).

[33] B. Batistić and M. Robnik, Phys. Rev. E **88**, 052913 (2013).

[34] B. Batistić and M. Robnik, J. Phys. A: Math. Theor. **46**, 315102 (2013).

[35] B. Batistić, Č. Lozej, and M. Robnik, Nonlinear Phenom. Complex Syst. (Minsk) **21**, 225 (2018).

[36] B. Batistić, Č. Lozej, and M. Robnik, Phys. Rev. E **100**, 062208 (2019).

[37] B. Batistić, Č. Lozej, and M. Robnik, Nonlinear Phenom. Complex Syst. (Minsk) **23**, 17 (2020).

[38] E. J. Heller and S. Tomsovic, Phys. Today **46**(7), 38 (1993).

[39] V. Lopac, I. Mrkonjić, and D. Radić, Phys. Rev. E **59**, 303 (1999).

[40] H. Makino, T. Harayama, and Y. Aizawa, Phys. Rev. E **63**, 056203 (2001).

[41] V. Lopac, I. Mrkonjić, and D. Radić, Phys. Rev. E **64**, 016214 (2001).

[42] J. Chen, L. Mohr, H.-K. Zhang, and P. Zhang, Chaos **23**, 043137 (2013).

[43] L. Bunimovich, H.-K. Zhang, and P. Zhang, Commun. Math. Phys. **341**, 781 (2016).

[44] L. A. Bunimovich, G. Casati, T. Prosen, and G. Vidmar, Exp. Math. **1**, 10 (2019).

[45] M. V. Berry, Eur. J. Phys. **2**, 91 (1981).

[46] M. Robnik, J. Dobnikar, A. Rapisarda, T. Prosen, and M. Petkovšek, J. Phys. A: Math. Gen. **30**, L803 (1997).

[47] E. Vergini and M. Saraceno, Phys. Rev. E **52**, 2204 (1995).

[48] Č. Lozej, Ph.D. Thesis, University of Maribor, 2020.

[49] J. Tualle and A. Voros, Chaos Solitons Fractals **5**, 1085 (1995).

[50] A. Bäcker, S. Fürstberger, and R. Schubert, Phys. Rev. E **70**, 036204 (2004).

[51] M. Robnik, J. Phys. A: Math. Gen. **16**, 3971 (1983).

[52] M. Robnik, J. Phys. A: Math. Gen. **17**, 1049 (1984).

[53] F. Borgonovi, F. M. Izrailev, L. F. Santos, and V. G. Zelevinsky, Phys. Rep. **626**, 1 (2016).

[54] T. A. Brody, Lett. Nuovo Cimento **7**, 482 (1973).

[55] T. A. Brody, J. Flores, J. B. French, P. A. Mello, A. Pandey, and S. S. M. Wong, Rev. Mod. Phys. **53**, 385 (1981).

[56] R. S. MacKay and J. D. Meiss, Phys. Rev. A **37**, 4702 (1988).

[57] G. Casati and T. Prosen, Physica D **131**, 293 (1999).